International Journal of Engineering and Applied Sciences (IJEAS)
ISSN: 2394-3661, Volume-4, Issue-7, July 2017

Study on the Exact Solution For Natural Frequencies and Mode Shapes of the Longitudinal-Vibration Conic Rod Carrying Arbitrary Concentrated Elements

Jia-Jang Wu

***Abstract*— In this paper, a conic rod carrying arbitrary concentrated elements is called the conic rod system. First of all, the equation of motion for the longitudinal free vibration of a conic rod is transformed into a Bessel equation, and then the exact displacement function in terms of the Bessel functions is obtained. Next, based on the equations for compatibility of deformations and those for equilibrium of longitudinal forces at each attaching point (including the two ends of entire bar) between the concentrated elements and the conic rod, a characteristic equation of the form [H]{C}= {0} is obtained. Now, the natural frequencies of the conic rod system can be determined from the determinant equation |H| = 0, and the associated column vector for the integration constants, {C}, corresponding to each natural frequency, can be obtained from the simultaneous equation [H]{C}= {0}. The substitution of the last integration constants into the displacement functions of all the associated rod segments will produce the corresponding mode shape of the entire conic rod system. Finally, the important factors affecting the longitudinal vibration characteristics of a conic rod system will be investigated. To confirm the reliability of the presented technique, in this research, the exact solutions obtained from the presented technique were compared with the numerical solutions obtained from the conventional finite element method (FEM). Good agreement is achieved.**

***Index Terms*— concentrated elements, conic rod, exact solution, longitudinal-vibration.**

I. INTRODUCTION

For convenience, in this paper, a conic rod with its longitudinal (lateral) surface generated by revolving an inclined straight line about its longitudinal axis is called the general conic rod (cf. Figure 1), and that generated by revolving an inclined curve about its longitudinal axis is called the specific conic rod (cf. Figure A1 in Appendix A). The main difference between the last two conic rods is that, the variation of cross-section area $A(x)$ is to take the form $A(x) = A_\ell (x/L_\ell)^2$ for the general conic rod (cf. Figure 1) and $A(x) = (ax+b)^n$ for the specific conic rod (cf. Figure A1). In the last two expressions for $A(x)$, x denotes the longitudinal axis of the conic rod with origin at the tip (or left) end, A_ℓ represents the cross-sectional area of the general conic rod at $x = L_\ell$ with the subscript ℓ denoting the *larger* end of the rod, while a, b and n are constants (with $b \neq 0$). Although one can obtain the exact solution for the natural frequencies and associated mode shapes of transverse (bending) vibration of the general conic rods from the existing literature [1,2], the exact solution for those of longitudinal (tension/compression) vibration of the foregoing general conic rods is not yet obtained to the authors' knowledge. In spite of the last fact, the exact solution for natural frequencies (without mode shapes) of the longitudinal vibration of specific conic rods with special area variations has been reported in [3, 4, 5]. In references [3-5], the exact solution for natural frequencies (without mode shapes) of longitudinal free vibration of a specific conic rod is obtained by using appropriate transformations to reduce its equation of motion to the analytically solvable standard differential equation of the form dependent upon the specific area variation $A(x) = (a+bx)^n$. From the foregoing literature review, one finds that the exact solution for the natural frequencies and associated mode shapes of the most practical general conic rod (cf. Figure 1) is not yet presented. Therefore, this paper tries to present it, particularly for those of a general conic rod carrying arbitrary point masses or/and linear springs.

First of all, the equation of motion for the longitudinal-vibration of general conic rod is transformed into the Bessel equation so that the exact solution for the axial displacements of the conic rod can easily be obtained. It has been found that all Bessel functions for the exact axial displacements of the general conic rod can be replaced by the trigonometric functions so that the difficulty arising from differentiations and computer coding of the Bessel functions is significantly reduced. Next, the equations for compatibility of deformations and equilibrium of forces at a typical intermediate node i connecting the conic rod segments (i) and (i+1), and those at the two ends of the entire conic rod are established. Based on these equations and the prescribed boundary conditions, corresponding to each of the trial natural frequencies, a characteristic equation for all the conic rod segments, , is obtained, where {C} is a column vector composed of the integration constants of all conic rod segments and [H] is a square matrix composed of the associated coefficients. Using the half-interval method [6], one may obtain the natural frequency of the vibrating system from the determinant equation |H| = 0, and, in turn, the associated integration constants from the characteristic equation . The substitution of the last integration constants into the associated displacement function for each of the conic rod segments will determine the corresponding mode shape. Repetition of the foregoing procedure q times will yield q natural frequencies and associated mode shapes. Finally, the influence of taper ratio, classical and non-classical boundary

Jia-Jang Wu, Department of Marine Engineering, National Kaohsiung Marine University, Kaohsiung City, Taiwan, +886+7+8100888ext5230

(supporting) conditions, and kind (and distribution) of concentrated elements (point masses and linear springs) on the free vibration characteristics of the conic rod is studied. In addition to the exact method presented in this paper, the conventional finite element method (FEM) is also used to tackle the same problem. To this end, the entire conic rod is replaced by a stepped rod composed of a number of uniform rod elements with identical element lengths and equal-increment (or -decrement) diameters. It has been found that the numerical results of the presented exact method and those of FEM are in good agreement.

For convenience, in this paper, a conic rod without any attachments is called the bare rod and the one carrying any concentrated elements is called the loaded rod. Besides, all conic rods indicate the general ones unless particularly mentioned..

II. Bessel Equation for the Longitudinal Vibration of a Conic Rod

For a non-uniform rod performing longitudinal (axial) free vibrations, its equation of motion takes the form [7]

$$\frac{\partial}{\partial x}\left[EA(x)\frac{\partial u(x,t)}{\partial x}\right]-\rho A(x)\frac{\partial^2 u(x,t)}{\partial t^2}=0 \qquad (1)$$

where ρ and E are mass density and Young's modulus of the rod material, respectively, $A(x)$ is the cross-sectional area of the rod at position x, and $u(x,t)$ is the axial displacement of the rod at position x and time t. For the truncated general conic rod as shown in Figure 1, x is the axial coordinate with its origin o at the tip end of the complete wedge rod. It is evident that revolution of the inclined straight line $\overline{AB}$ about the horizontal x-axis will generate its longitudinal (lateral) surface.

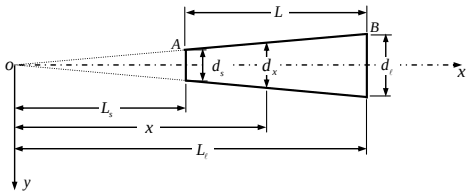

Figure 1 The coordinate system for a truncated general conic rod with diameter d_ℓ at its larger end, diameter d_s at its smaller end and length $L=L_\ell-L_s$. (Note that $d_s/L_s=d_\ell/L_\ell$.)

If d_ℓ and d_s denote the diameters of the larger end and smaller end of the truncated conic rod (cf. Figure 1), respectively, then the diameter for the cross-section located at position x is given by

$$d_x=\left(\frac{x}{L_\ell}\right)d_\ell \qquad (2)$$

with L_ℓ denoting the total length of the complete wedge rod, and the cross-sectional area $A(x)$ is given by

$$A(x)=\frac{\pi d_x^2}{4}=\left(\frac{x}{L_\ell}\right)^2 A_\ell \qquad (3)$$

where A_ℓ is the cross-sectional area of the larger end of the rod located at $x=L_\ell$ and is given by

$$A_\ell=\frac{\pi d_\ell^2}{4} \qquad (4)$$

For free vibrations, one has

$$u(x,t)=U(x)e^{j\omega t} \qquad (5)$$

where $U(x)$ denotes the amplitude of $u(x,t)$, ω denotes the angular natural frequency of conic rod and $j=\sqrt{-1}$.

Substituting Equations (4) and (5) into Equation (1), one obtains

$$\frac{d}{dx}\left[x^2\frac{dU(x)}{dx}\right]+\beta^2x^2U(x)=0 \qquad (6)$$

where

$$\beta^2=\frac{\rho\omega^2}{E} \qquad (7)$$

Equation (6) is a Bessel equation with its solution composed of the Bessel functions.

III. Displacement Function for the Conic Rod

From reference [8], one sees that the solution for the next differential equation

$$(\chi^{\mathrm{r}}y')'+(a\chi^{\mathrm{s}}+b\chi^{\mathrm{r}-2})y=0 \qquad (8)$$

is given by

$$y=\chi^{\alpha}[c_1J_v(\lambda\chi^{\gamma})+c_2Y_v(\lambda\chi^{\gamma})] \qquad (9)$$

where the primes (') in Eqration (8) denote the differentiations with respect to χ and the parameters in Equation (9) are given by

$$\alpha=\frac{1-\mathrm{r}}{2},\ \gamma=\frac{2-\mathrm{r}+\mathrm{s}}{2},\ \lambda=\frac{2\sqrt{|a|}}{2-\mathrm{r}+\mathrm{s}},\ v=\frac{\sqrt{(1-\mathrm{r})^2-4b}}{2-\mathrm{r}+\mathrm{s}} \qquad (10a,b,c,d)$$

Comparing Equation (8) with Equation (6), one sees that

$$\chi=x,\ y=U,\ \mathrm{r}=2,\ b=0,\ a=\beta^2,\ s=2 \qquad (11)$$

Thus, from Equation (9), one obtains the solution of Equation (6) to be

$$U(x)=x^{\alpha}[c_1J_v(\lambda x^{\gamma})+c_2Y_v(\lambda x^{\gamma})] \qquad (12)$$

where $J_v(z)$ and $Y_v(z)$ are the first kind and second kind Bessel functions of order v [8].

Now, from Equations (10) and (11), one has

$$\alpha=-\tfrac{1}{2},\ \gamma=1,\ \lambda=\beta,\ v=1/2 \qquad (13a,b,c,d)$$

Substituting the last parameters into Equation (12) and using the relationship $Y_{1/2}(z)\propto J_{-1/2}(z)$ [8], one has

$$U_\tau(z_\tau)=\beta_\tau^{1/2}z_\tau^{-1/2}[C_1^{(\tau)}J_{1/2}(z_\tau)+C_2^{(\tau)}J_{-1/2}(z_\tau)]\ (\tau=1,2,3,\ldots) \qquad (14)$$

where

$$z_\tau=\beta_\tau x \qquad (15a)$$

$$\beta_\tau^2=\frac{\rho\omega_\tau^2}{E} \qquad (15b)$$

In Equations (14) and (15), the subscript τ refers to the τ -th vibrating mode of the conic rod, while $C_1^{(\tau)}$ and $C_2^{(\tau)}$ denote the two corresponding integration constants determined by the associated boundary conditions.

IV. Boundary Conditions

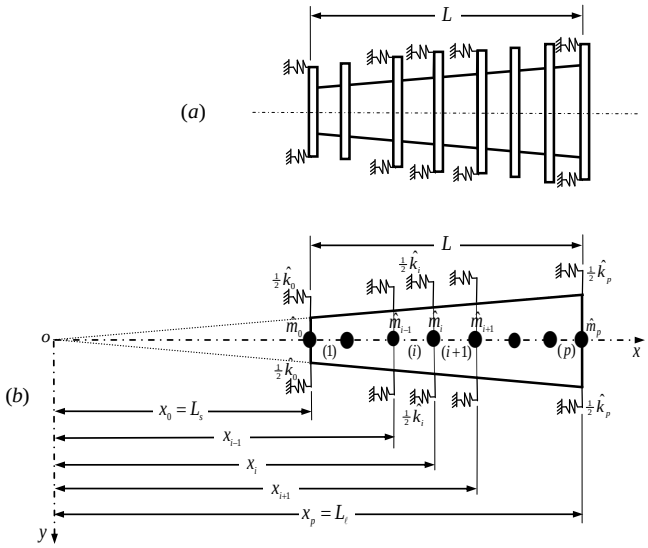

Figure2 (a) A free-free truncated conic rod is supported by a number of collars (or flanges) and linear springs; (b) The mathematical model for the last conic rod is composed of p conic rod segments (denoted by (1), (2),…, (i), …, (p)), and carrying one point mass $\hat{m}_i$ and one linear spring $\hat{k}_i$ at node i ($i = 0, 1, 2, \ldots, p$).

Figure 2(a) shows a free-free truncated conic rod supported by a number of collars (or flanges) and linear springs, and Figure 2(b) shows its mathematical model composed of p conic rod segments (denoted by (1), (2),…, (i), …, (p)) and carrying one point mass $\hat{m}_i$ and one linear spring $\hat{k}_i$ at node i ($i = 0, 1, 2, \ldots, p$). The compatibility of displacements and equilibrium of forces at the arbitrary intermediate node i located at $x = x_i$ require that

$$U_{\tau,i}(z_{\tau,i}) = U_{\tau,i+1}(z_{\tau,i}) \tag{16a}$$

$$EA_i U'_{\tau,i}(z_{\tau,i}) = EA_i U'_{\tau,i+1}(z_{\tau,i}) + (\omega^2 \hat{m}_i - \hat{k}_i) U_{\tau,i}(z_{\tau,i}) \tag{16b}$$

where

$$z_{\tau,i} = \beta_\tau x_i \tag{17a}$$

$$A_i = (x_i / L_\ell)^2 A_\ell \tag{17b}$$

The boundary condition for the left end of the entire conic rod is

$$EA_0 U'_{\tau,1}(z_{\tau,0}) + (\omega^2 \hat{m}_0 - \hat{k}_0) U_{\tau,1}(z_{\tau,0}) = 0 \tag{18}$$

where

$$z_{\tau,0} = \beta_\tau x_0 = \beta_\tau L_s \tag{19a}$$

$$A_0 = (x_0 / L_\ell)^2 A_\ell = (L_s / L_\ell)^2 A_\ell \tag{19b}$$

Similarly, the boundary condition for the right end of the entire conic rod is

$$EA_p U'_{\tau,p}(z_{\tau,p}) - (\omega^2 \hat{m}_p - \hat{k}_p) U_{\tau,p}(z_{\tau,p}) = 0 \tag{20}$$

with

$$z_{\tau,p} = \beta_\tau x_p = \beta_\tau L_\ell \tag{21a}$$

$$A_p = (x_p / L_\ell)^2 A_\ell = (L_\ell / L_\ell)^2 A_\ell = A_\ell \tag{21b}$$

Equations (18) and (20) are the non-classical boundary conditions. As to the general classical boundary conditions (without any attachments at both ends of the rod), they are given by

$$U'_{\tau,1}(z_{\tau,0}) = 0,\ U'_{\tau,p}(z_{\tau,p}) = 0 \quad \text{(for F-F rod)} \tag{22a,b}$$

$$U_{\tau,1}(z_{\tau,0}) = 0,\ U_{\tau,p}(z_{\tau,p}) = 0 \quad \text{(for C-C rod)} \tag{23a,b}$$

$$U_{\tau,1}(z_{\tau,0}) = 0,\ U'_{\tau,p}(z_{\tau,p}) = 0 \quad \text{(for C-F rod)} \tag{24a,b}$$

$$U'_{\tau,1}(z_{\tau,0}) = 0,\ U_{\tau,p}(z_{\tau,p}) = 0 \quad \text{(for F-C rod)} \tag{25a,b}$$

In Equations (22)-(25), the capital letters F and C denote the abbreviations of *free* and *clamped* ends, respectively. Besides, the symbol $U_{\tau,1}(z_{\tau,0})$ and $U'_{\tau,1}(z_{\tau,0})$ denote the displacement and its first derivative of the 1st rod segment at node 0 (cf. Figure 2), respectively. Similarly, $U_{\tau,p}(z_{\tau,p})$ and $U'_{\tau,p}(z_{\tau,p})$ denote those of the final (p-th) rod segment at node p, respectively.

V. Determination of Exact Natural Frequencies and Mode Shapes

From Equation (14), one obtains the displacement function for the i-th conic rod segment to be

$$U_{\tau,i}(z_{\tau,i}) = \beta_\tau^{1/2} z_{\tau,i}^{-1/2} [C_{1,i}^{(\tau)} J_{1/2}(z_{\tau,i}) + C_{2,i}^{(\tau)} J_{-1/2}(z_{\tau,i})] \tag{26a}$$

Thus, the first derivative of $U_{\tau,i}(z_{\tau,i})$ is given by

$$\begin{aligned} &U'_{\tau,i}(z_{\tau,i}) \\ &= \beta_\tau^{3/2} z_{\tau,i}^{-1/2} \{-\tfrac{1}{2} z_{\tau,i}^{-1} [C_{1,i}^{(\tau)} J_{1/2}(z_{\tau,i}) + C_{2,i}^{(\tau)} J_{-1/2}(z_{\tau,i})] + \\ &\qquad [C_{1,i}^{(\tau)} J'_{1/2}(z_{\tau,i}) + C_{2,i}^{(\tau)} J'_{-1/2}(z_{\tau,i})]\} \end{aligned} \tag{26b}$$

where

$$J'_\nu(z) = dJ_\nu / dz \quad (\nu = 1/2 \text{ or } -1/2) \tag{27}$$

It has been found that much difficulty concerning the differentiations and computer coding for the foregoing Bessel functions will be removed if the following relationships [9] are used

$$J_{1/2}(z) = \left(\frac{2}{\pi z}\right)^{1/2} \sin z \tag{28a}$$

$$J_{-1/2}(z) = \left(\frac{2}{\pi z}\right)^{1/2} \cos z \tag{28b}$$

From the last two expressions, one obtains

$$J'_{1/2}(z) = \frac{d}{dz}[J_{1/2}(z)] = \left(\frac{2}{\pi}\right)^{1/2} \{-\tfrac{1}{2} z^{-3/2} \sin z + z^{-1/2} \cos z\} \tag{29a}$$

$$J'_{-1/2}(z) = \frac{d}{dz}[J_{-1/2}(z)] = \left(\frac{2}{\pi}\right)^{1/2} (-\tfrac{1}{2} z^{-3/2} \cos z - z^{-1/2} \sin z) \tag{29b}$$

Now, the exact natural frequencies and the associated mode shapes of a conic rod with various boundary conditions are determined in the following.

A. *For the free-free (F-F) conic rod*

For the F-F conic rod as shown in Figure 2, the substitutions of Equations (26a) and (26b) into Equation (18) lead to

$$\begin{aligned} &C_{1,1}^{(\tau)} \{[-\tfrac{1}{2} \beta_\tau z_{\tau,0}^{-1} + f_{\tau,0}] J_{1/2}(z_{\tau,0}) + \beta_\tau J'_{1/2}(z_{\tau,0})\} \\ &+ C_{2,1}^{(\tau)} \{[-\tfrac{1}{2} \beta_\tau z_{\tau,0}^{-1} + f_{\tau,0}] J_{-1/2}(z_{\tau,0}) + \beta_\tau J'_{-1/2}(z_{\tau,0})\} = 0 \end{aligned} \tag{30}$$

where

$$f_{\tau,0} = (\omega_\tau^2 \hat{m}_0 - \hat{k}_0) / (EA_0) \tag{31}$$

Similarly, substituting Equations (26a) and (26b) into Equations (16a) and (16b), respectively, one obtains

$$C_{1,i}^{(\tau)} J_{1/2}(z_{\tau,i}) + C_{2,i}^{(\tau)} J_{-1/2}(z_{\tau,i}) - C_{1,i+1}^{(\tau)} J_{1/2}(z_{\tau,i}) - C_{2,i+1}^{(\tau)} J_{-1/2}(z_{\tau,i}) = 0 \tag{32}$$

$$\begin{aligned}&C_{1,i}^{(\tau)}\{[-\tfrac{1}{2}\beta_\tau z_{\tau,i}^{-1}-f_{\tau,i}]J_{1/2}(z_{\tau,i})+\beta_\tau J'_{1/2}(z_{\tau,i})]\}\\&+C_{2,i}^{(\tau)}\{[-\tfrac{1}{2}\beta_\tau z_{\tau,i}^{-1}-f_{\tau,i}]J_{-1/2}(z_{\tau,i})+\beta_\tau J'_{-1/2}(z_{\tau,i})\}\\&+C_{1,i+1}^{(\tau)}\beta_\tau[\tfrac{1}{2}z_{\tau,i}^{-1}J_{1/2}(z_{\tau,i})-J'_{1/2}(z_{\tau,i})]\\&+C_{2,i+1}^{(\tau)}\beta_\tau[\tfrac{1}{2}z_{\tau,i}^{-1}J_{-1/2}(z_{\tau,i})-J'_{-1/2}(z_{\tau,i})]=0\end{aligned}\tag{33}$$

where

$$f_{\tau,i}=(\omega_\tau^2\hat{m}_i-\hat{k}_i)/(EA_i)\tag{34}$$

Finally, the substitutions of Equations (26a) and (26b) into Equation (20) lead to

$$\begin{aligned}&C_{1,p}^{(\tau)}\{[-\tfrac{1}{2}\beta_\tau z_{\tau,p}^{-1}-f_{\tau,p}]J_{1/2}(z_{\tau,p})+\beta_\tau J'_{1/2}(z_{\tau,p})\}\\&+C_{2,p}^{(\tau)}\{[-\tfrac{1}{2}\beta_\tau z_{\tau,p}^{-1}-f_{\tau,p}]J_{-1/2}(z_{\tau,p})+\beta_\tau J'_{-1/2}(z_{\tau,p})\}=0\end{aligned}\tag{35}$$

where

$$f_{\tau,p}=(\omega_\tau^2\hat{m}_p-\hat{k}_p)/(EA_p)\tag{36}$$

Based on Equations (30), (32), (33) and (35), one obtains

$$[H]_{\bar{n}\times\bar{n}}\{C\}_{\bar{n}\times 1}=0\tag{37}$$

where $\{C\}_{\bar{n}\times 1}$ is a $\bar{n}\times 1$ column vector composed of $\bar{n}=2p$ integration constants for the τ-th mode shape of the p rod segments, $C_{1,i}^{(\tau)}$ and $C_{2,i}^{(\tau)}$ ($i=1,\ldots,i,\ldots,p$), i.e.,

$$\{C\}_{\bar{n}\times 1}=[C_{1,1}^{(\tau)}\quad C_{2,1}^{(\tau)}\quad\cdots\quad C_{1,i}^{(\tau)}\quad C_{2,i}^{(\tau)}\quad\cdots\quad C_{1,p}^{(\tau)}\quad C_{2,p}^{(\tau)}]^T\tag{38}$$

and $[H]_{\bar{n}\times\bar{n}}$ is a $\bar{n}\times\bar{n}$ (with $\bar{n}=2p$) square matrix with its non-zero coefficients determined by:

$$H_{1,1}=[-\tfrac{1}{2}\beta_\tau z_{\tau,0}^{-1}+f_{\tau,0}]J_{1/2}(z_{\tau,0})+\beta_\tau J'_{1/2}(z_{\tau,0})\tag{39a}$$

$$H_{1,2}=[-\tfrac{1}{2}\beta_\tau z_{\tau,0}^{-1}+f_{\tau,0}]J_{-1/2}(z_{\tau,0})+\beta_\tau J'_{-1/2}(z_{\tau,0})\tag{39b}$$

$$H_{2i,2(i-1)+1}=J_{1/2}(z_{\tau,i}),\ H_{2i,2(i-1)+2}=J_{-1/2}(z_{\tau,i})\tag{40a,b}$$

$$H_{2i,2(i-1)+3}=-J_{1/2}(z_{\tau,i}),\ H_{2i,2(i-1)+4}=-J_{-1/2}(z_{\tau,i})\tag{40c,d}$$

$$H_{2i+1,2(i-1)+1}=[-\tfrac{1}{2}\beta_\tau z_{\tau,i}^{-1}-f_{\tau,i}]J_{1/2}(z_{\tau,i})+\beta_\tau J'_{1/2}(z_{\tau,i})\tag{41a}$$

$$H_{2i+1,2(i-1)+2}=[-\tfrac{1}{2}\beta_\tau z_{\tau,i}^{-1}-f_{\tau,i}]J_{-1/2}(z_{\tau,i})+\beta_\tau J'_{-1/2}(z_{\tau,i})\tag{41b}$$

$$H_{2i+1,2(i-1)+3}=\beta_\tau[\tfrac{1}{2}z_{\tau,i}^{-1}J_{1/2}(z_{\tau,i})-J'_{1/2}(z_{\tau,i})]\tag{41c}$$

$$H_{2i+1,2(i-1)+4}=\beta_\tau[\tfrac{1}{2}z_{\tau,i}^{-1}J_{-1/2}(z_{\tau,i})-J'_{-1/2}(z_{\tau,i})]\tag{41d}$$

$$H_{\bar{n},\bar{n}-1}=[-\tfrac{1}{2}\beta_\tau z_{\tau,p}^{-1}-f_{\tau,p}]J_{1/2}(z_{\tau,p})+\beta_\tau J'_{1/2}(z_{\tau,p})\tag{42a}$$

$$H_{\bar{n},\bar{n}}=[-\tfrac{1}{2}\beta_\tau z_{\tau,p}^{-1}-f_{\tau,p}]J_{-1/2}(z_{\tau,p})+\beta_\tau J'_{-1/2}(z_{\tau,p})\tag{42b}$$

It is noted that Equations (40) and (41) are required only if $p>1$ and $i\le(p-1)$ with p and i denoting the total number of rod segments and numbering of the intermediate nodes, respectively. For the special case of $p=1$, only Equations (39) and (42) are required for the determination of natural frequencies and associated mode shapes. Besides, in Equations (39)-(42), the values of $J_v(z_{\tau,i})$ and $J'_v(z_{\tau,i})$ with $v=\pm\frac{1}{2}$ and $i=0,1,2,\ldots,p$ are determined by Equations (28) and (29). Non-trivial solution of Equation (37) requires that its coefficient determinant is equal to zero, i.e.,

$$|H|=0\tag{43}$$

Equation (43) is the frequency equation for the F-F conic rod carrying $p+1$ point masses $\hat{m}_i$ and $p+1$ linear springs $\hat{k}_i$ ($i=0,1,2,\ldots,p$). In general, the half-interval method [6] is used to find the natural frequencies of the vibrating system, ω_τ ($\tau=1,2,3,\ldots$), one by one and then, with respect to each natural frequency ω_τ, one may determine the values of $C_{1,i}^{(\tau)}$ and $C_{2,i}^{(\tau)}$ ($i=1,2,\ldots,p$) from Equation (37). Finally, the substitution of the last integration constants into Equation (26a) will determine the corresponding natural mode shape of the entire conic rod $U_\tau(x)$. Since the values of point masses $\hat{m}_i$ and linear springs $\hat{k}_i$ are arbitrary including zero, the foregoing formulation is available for arbitrary cases of the free-free conic rod including the bare one.

For the special case of only one rod segment (i.e., $p=1$), Equation (37) reduces to

$$[H]_{2\times 2}\{C\}_{2\times 1}=0\tag{44}$$

where

$$\{C\}_{2\times 1}=[C_{1,1}^{(\tau)}\quad C_{2,1}^{(\tau)}]\tag{45a}$$

$$[H]_{2\times 2}=\begin{bmatrix}H_{1,1} & H_{1,2}\\ H_{2,1} & H_{2,2}\end{bmatrix}\tag{45b}$$

In Equation (45b), the coefficients $H_{1,1}$ and $H_{1,2}$ are the same as those given by Equations (39a) and (39b), while those $H_{2,1}$ and $H_{2,2}$ may be obtained from Equations (42a) and (42b) by letting $p=1$ and $\bar{n}=2p=2$. The results are

$$H_{2,1}=[-\tfrac{1}{2}\beta_\tau z_{\tau,1}^{-1}-f_{\tau,1}]J_{1/2}(z_{\tau,1})+\beta_\tau J'_{1/2}(z_{\tau,1})\tag{46a}$$

$$H_{2,2}=[-\tfrac{1}{2}\beta_\tau z_{\tau,1}^{-1}-f_{\tau,1}]J_{-1/2}(z_{\tau,1})+\beta_\tau J'_{-1/2}(z_{\tau,1})\tag{46b}$$

where

$$z_{\tau,1}=\beta_\tau x_\ell=\beta_\tau L_\ell\tag{47}$$

B. *For the clamped-clamped (C-C) conic rod*

If the left and right ends of the conic rod as shown in Figure 2 are clamped, then the effects of the two point masses and two linear springs at the last two ends (i.e., $\hat{m}_0$, $\hat{m}_p$, $\hat{k}_0$ and $\hat{k}_p$) are nil. In such a case, the boundary conditions of the conic rod are the same as the classical ones given by Equations (23a) and (23b). The substitution of Equation (26a) into Equations (23a) and (23b), respectively, leads to

$$C_{1,1}^{(\tau)}J_{1/2}(z_{\tau,0})+C_{2,1}^{(\tau)}J_{-1/2}(z_{\tau,0})=0\tag{48a}$$

$$C_{1,p}^{(\tau)}J_{1/2}(z_{\tau,p})+C_{2,p}^{(\tau)}J_{-1/2}(z_{\tau,p})=0\tag{48b}$$

Therefore, the formulation presented in the last subsection 5.1 is also available for the free vibration analysis of the C-C conic rod, if the coefficients relating to the boundary conditions, given by Equations (39a,b) and (42a,b), are respectively replaced by

$$H_{1,1}=J_{1/2}(z_{\tau,0}),\ H_{1,2}=J_{-1/2}(z_{\tau,0})\tag{49a,b}$$

$$H_{\bar{n},\bar{n}-1}=J_{1/2}(z_{\tau,p}),\ H_{\bar{n},\bar{n}}=J_{-1/2}(z_{\tau,p})\tag{50a,b}$$

C. *For the clamped-free (C-F) or free-clamped (F-C) conic rod*

The formulation presented in subsection 5.1 is also available for the free vibration analysis of the clamped-free (C-F) or free-clamped (F-C) conic rod, if the following actions are taken: (i) The coefficients $H_{1,1}$ and $H_{1,2}$ given by Equations (39a,b) must be used if the left end is free, but those given by Equations (49a,b) must be used if the left end is clamped. (ii) The coefficients $H_{\bar{n},\bar{n}-1}$ and $H_{\bar{n},\bar{n}}$ given by Equations (42a,b) must be used if the right end is free, but those given by Equations (50a,b) must be used if the right end is clamped. It is noted that, for the classical boundary conditions, $\hat{m}_0=\hat{k}_0=0$ and $\hat{m}_p=\hat{k}_p=0$.

VI. Free Longitudinal Vibration Analysis of a Conic Rod by FEM

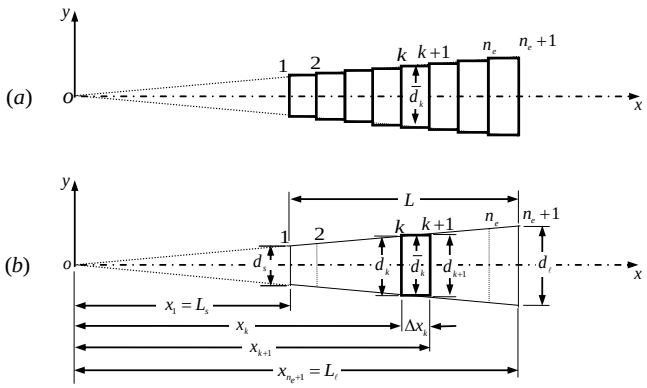

Figure 3 The FEM model: (a) the truncated conic rod (with diameter d_s at small end and diameter d_ℓ at large end) is replaced by n_e uniform circular rod elements; (b) the average diameter $\bar{d}_k$ ($k = 1,2,3,\ldots,n_e$) for the *k*-th uniform circular rod element is determined by $\bar{d}_k = (d_k + d_{k+1})/2$.

In order to use the conventional FEM to tackle the current problem, the first step is to replace the conic rod by a stepped one composed of n_e uniform circular rod elements as shown in Figure 3(a). The average diameter of the *k*-th uniform rod element is determined by (cf. Figure 3(b))

$$\bar{d}_k = (d_k + d_{k+1})/2 \tag{51}$$

where d_k and d_{k+1} are the diameters of cross-sections of the original conic rod located at the two ends of the *k*-th uniform rod segment, respectively, and are given by (cf. Figure 3(b))

$$d_k = \left(\frac{x_k}{L_\ell}\right) d_\ell \,,\; d_{k+1} = \left(\frac{x_{k+1}}{L_\ell}\right) d_\ell \tag{52a,b}$$

Thus, the average cross-sectional area of the *i*-th uniform rod element is given by

$$\bar{A}_k = \pi \bar{d}_k^2 / 4 \tag{53}$$

The total mass m_k and length ℓ_k of the *k*-th uniform rod element are determined by

$$m_k = \frac{1}{3} \cdot \rho \left(\frac{\pi\, d_{k+1}^2}{4} x_{k+1} - \frac{\pi\, d_k^2}{4} x_k \right) \tag{54}$$

$$\ell_k = \Delta x_k = L / n_e \tag{55}$$

Based on the foregoing information for the *k*-th uniform rod element ($k = 1,2,3,\ldots,n_e$) and Young's modulus of the rod material, one may obtain the mass matrix and stiffness matrix of each uniform rod element from [10]

$$[m]_k = m_k \begin{bmatrix} \frac{1}{3} & \frac{1}{6} \\ \frac{1}{6} & \frac{1}{3} \end{bmatrix},\; [k]_k = \left(\frac{E\bar{A}_k}{\ell_k} \right) \begin{bmatrix} 1 & -1 \\ -1 & 1 \end{bmatrix} \tag{56a,b}$$

Assembly of the elemental mass and stiffness matrices for each of the uniform rod elements yields the overall mass matrix [*m*] and overall stiffness matrix [*k*] of the entire conic rod. If there exist a point mass $\hat{m}_k$ and a linear spring $\hat{k}_k$ at $x = x_k$, then $\hat{m}_k$ and $\hat{k}_k$ must be added to the *k*-th diagonal coefficient of the overall mass matrix [*m*] and that of the overall stiffness matrix [*k*], respectively, i.e., one must replace m_{kk} by $m_{kk} + \hat{m}_k$ and k_{kk} by $k_{kk} + \hat{k}_k$. Finally, imposing the specified boundary condition of the entire conic rod and solving the resulting characteristic equation, one determines the natural frequencies and the corresponding mode shapes of the conic rod.

VII. Numerical Results and Discussions

Unless particularly mentioned, the dimensions of the conical rod (cf. Figure 1) studied in this paper are the same as those of the rod with taper ratio $\bar{\alpha} = d_\ell / L_h = 0.01$ (i.e., case 2) shown in Table 1: length of the complete conic rod $L_\ell = 5.0$ m, length truncated $L_s = 3.0$ m, actual length of the conic rod $L = L_\ell - L_s = 2.0$ m, diameter at smaller end $d_s = 0.03$ m, diameter at larger end $d_\ell = 0.05$ m, Young's modulus $E = 2.068 \times 10^{11}$ N/m^2 and mass density $\rho = 7850$ kg/m^3 . It is noted that the foregoing dimensions must satisfy the relationship $\bar{\alpha} = d_s / L_s = d_\ell / L_\ell$, with $\bar{\alpha}$ denoting the taper ratio. For convenience, two reference parameters are introduced in this paper, one is *reference mass* defined by $m^* = \frac{1}{3}\rho(A_\ell L_\ell - A_s L_s)$ and the other is *reference stiffness* defined by $k^* = EA_{ave}/L$, where $A_\ell = \pi d_\ell^2/4$ and $A_s = \pi d_s^2/4$ denote the cross-sectional areas at the larger end and smaller end of the conic rod, respectively, and $A_{ave} = (A_\ell + A_s)/2$ is the average cross-sectional area of the conic rod. All the other symbols have been defined previously for Figure 1. It is evident that m^* and k^* represents the total mass and average stiffness of the conic rod, respectively. Based on the foregoing dimensions and physical constants of the conic rod, one obtains $m^* = \frac{1}{3}\rho(A_\ell L_\ell - A_s L_s) =$ 20.140226 kg and $k^* = EA_{ave}/L =$ 1.3805728 $\times 10^8$ N/m with $\pi = 3.1415926$ being used.

A. Validation of the presented theory

One of the reasonable techniques to confirm the reliability of the presented theory is to reduce the taper ratio $\bar{\alpha} = d_\ell / L_\ell$ of the conic rod gradually and to see whether or not its lowest several natural frequencies converge to the corresponding ones of the associated uniform rod. To this end, the lowest five natural frequencies of a conic rod with five taper ratios, $\bar{\alpha}$ = 0.02, 0.01, 0.005, 0.0025 and 0.0010, are studied (cf. Figure 4). Corresponding to each taper ratio (designated as cases 1, 2, 3, 4 and 5, respectively), the dimensions of the conic rod are shown in Table 1. It is noted that the diameter of the (right) larger end, $d_\ell = 0.05$ m, and the rod length $L = L_\ell - L_s = 2.0$ m are kept unchanged as one may see from Figure 4. Besides, the relationship $\bar{\alpha} = d_s / L_s = d_\ell / L_\ell$ is hold true for all five cases. The lowest five natural frequencies for the five cases of the conic rod in four boundary conditions (BC's) are shown in Table 2 by using single rod segment (i.e., *p* = 1), in which the capital letters, F and C, denote the free and clamped ends of the conic rod, respectively. From Table 2 one sees that: (i) When the taper ratio $\bar{\alpha}$ reduces from 0.02 (case 1) to 0.001(case 5), the lowest five natural frequencies, ω_τ ($\tau = 1-5$) (rad/sec), of the conic rod in either F-F, C-C, C-F or F-C BC's converge to the corresponding ones of the associated uniform rod with its exact natural frequencies obtained from the formulas given in Appendix B at end of this

paper. The above-mentioned exact natural frequencies are listed in Table 2 denoted by the bold-faced digits. (ii) For F-F and F-C rods, their lowest five natural frequencies decrease with the decrease of taper ratios $\bar{\alpha}$. This is a reasonable result, because the mass of each conic rod near its (left) free end increases significantly with the decrease of taper ratio $\bar{\alpha}$. (iii) The lowest five natural frequencies of the C-F rod increase with the decrease of taper ratio $\bar{\alpha}$. This is also a reasonable result, because the diameter of the (left) clamped end of the C-F rod increases with the decrease of its taper ratio $\bar{\alpha}$ and so does the longitudinal rigidity (EA_s) at its (left) clamped support. Although the total mass of the conic rod increases also, its influence is less than the above-mentioned longitudinal rigidity because most of the increased mass is near the (left) clamped end. (iv) For the uniform rod, the natural frequencies in C-F support conditions are the same as those in F-C conditions, however, this is not true for the conic rod, because the natural frequencies of the C-F conic rod are different from those of the F-C conic rod, and the larger the taper ratio $\bar{\alpha} = d_\ell / L_\ell$ the larger the divergence between them. (v) For any case of the five taper ratios $\bar{\alpha}$, the lowest five natural frequencies of the C-C conic rod are the same as those of the C-C uniform rod. This agrees with the results given in Table 1 of reference [4], in which, the lowest six natural frequencies of the two specific C-C conic rods with their longitudinal cross-sections shown in Figure A1 of this paper (in Appendix A) are very close to the lowest six ones of the associated C-C uniform rod. To confirm the reliability of the last results, the same problem is solved for the lowest five natural frequencies by using the conventional finite element method (FEM) with 50 rod elements (i.e., $n_e = 50$). The results for taper ratios $\bar{\alpha}$ = 0.02 and 0.001, respectively, are listed in the parentheses ( ) of Table 2. It is seen that that the lowest five natural frequencies of the C-C conic rod with $\bar{\alpha}$ = 0.02 are very close to the corresponding ones with $\bar{\alpha}$ = 0.001.

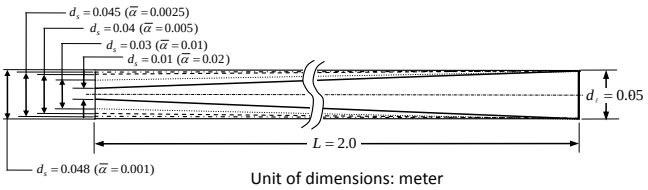

Figure 4 The profiles for longitudinal cross-sections of the conic rod with five different taper ratios (cf. Table 1).

Table 1 The dimensions of a general conic rod with five taper ratios ($\bar{\alpha} = d_\ell / L_\ell$). (Larger-end diameter $d_\ell = 0.05$ m and rod length $L = 2.0$ m are kept unchanged.)

Case	$\bar{\alpha} = d_\ell / L_\ell$	L_ℓ (m)	L_s (m)	d_s (m)	L (m)	d_ℓ (m)
1	0.02	2.5	0.5	0.01	2.0	0.05
2	**0.01**	**5.0**	**3.0**	**0.03**		
3	0.005	10.0	8.0	0.04		
4	0.0025	20.0	18.0	0.045		
5	0.001	50.0	48.0	0.048		
Uniform rod		—	—	0.05	2.0	0.05

Table 2 Influence of taper ratio ($\bar{\alpha} = d_\ell / L_\ell$) on the lowest five natural frequencies ω_τ (rad/sec) of the conic rods with various boundary conditions (Larger-end diameter $d_\ell = 0.05$ m and rod length $L = 2.0$ m are kept unchanged.)

BCS	CASE	$\bar{\alpha}$	Natural frequencies, ω_τ (rad/sec)				
			ω_1	ω_2	ω_3	ω_4	ω_5
F F	1	0.0200	9621.44	17200.61	24977.21	32866.11	40814.97
	2	0.0100	8268.95	16232.06	24259.13	32303.56	40355.09
	3	0.0050	8102.75	16145.02	24200.57	32259.50	40319.79
	4	0.0025	8071.38	16129.18	24190.00	32251.56	40313.44
	5	0.0010	8063.68	16125.33	24187.42	32249.64	40311.89
	***Uniform rod**		**8062.32**	**16124.64**	**24186.97**	**32249.29**	**40311.62**
C C	1	0.0200	8062.32 #8063.92	16124.65 (16135.50)	24186.97 (24223.00)	32249.30 (32334.41)	40311.62 (40477.74)
	2	0.0100	8062.32	16124.65	24186.97	32249.30	40311.62
	3	0.0050	8062.32	16124.65	24186.97	32249.30	40311.62
	4	0.0025	8062.32	16124.65	24186.97	32249.30	40311.62
	5	0.0010	8062.32 #8063.65	16124.65 (16135.26)	24186.97 (24222.79)	32249.30 (32334.24)	40311.62 (40477.59)
	***Uniform rod**		**8062.32**	**16124.64**	**24186.97**	**32249.29**	**40311.62**
C F	1	0.0200	1948.62	11645.66	19891.87	28030.50	36134.81
	2	0.0100	3244.86	11872.14	20024.36	28124.51	36207.72
	3	0.0050	3675.04	11983.63	20090.26	28171.38	36244.12
	4	0.0025	3860.82	12038.78	20123.08	28194.78	36262.30
	5	0.0010	3964.73	12071.66	20142.73	28208.79	36273.20
	***Uniform rod**		**4031.16**	**12093.48**	**20155.81**	**28218.13**	**36280.46**
F C	1	0.0200	6596.54	13740.14	21307.95	29088.76	36975.43
	2	0.0100	4894.20	12444.11	20370.84	28372.70	36400.99
	3	0.0050	4402.53	12228.01	20237.14	28276.35	36325.78
	4	0.0025	4204.92	12153.68	20192.05	28244.04	36300.62
	5	0.0010	4098.10	12116.13	20169.41	28227.85	36288.02
	***Uniform rod**		**4031.16**	**12093.48**	**20155.81**	**28218.13**	**36280.46**

* The exact natural frequencies of the uniform rod obtained from formulas in Appendix B.

Natural frequencies obtained from the conventional FEM using 50 rod elements ($n_e = 50$).

Although the lowest five natural frequencies of the C-C conic rod with $\bar{\alpha}$ = 0.02 are the same as the corresponding ones with $\bar{\alpha}$ = 0.001, obtained from the exact method presented in this paper, the associated mode shapes are different from each other as shown in Figures 5(a)-(e) for the 1st -5th modes, respectively. From Figure 5 one sees that the lowest five mode shapes of the C-C conic rod with taper ratio $\bar{\alpha}$ = 0.001 (denoted by the dashed curves, ---) look like those of a uniform rod, because this conic rod is very close to the uniform rod as one may see from Figure 4. However, the last statement is incorrect for the ones with $\bar{\alpha}$ = 0.02 (cf. the solid curved in Figure 5, —). From Figure 5 one sees that, for the solid curves (with $\bar{\alpha}$ = 0.02), the local maximum mode displacements $U_\tau(x)$ near the left end are much greater than those near the right end, because the diameter of the cross-section at left end of the conic rod is minimum and that at right end is maximum as shown in Figure 4. In spite of the fact that the lowest five mode shapes of the C-C conic rod with $\bar{\alpha}$ = 0.02 are much different from those with $\bar{\alpha}$ = 0.001, the locations of nodes for the corresponding mode shapes are identical as one may see from Figure 5, and this should be one of the reasons that the corresponding natural frequencies are identical. In other words, for a C-C conic rod, the effect of taper ratio $\bar{\alpha}$ is to change the envelopes of the amplitudes of the longitudinal mode displacements, as shown in Figure 6, and it does not affect the locations of the nodes of the corresponding mode shapes. Thus, the lowest five natural frequencies are not affected by its taper ratios. In Figure 6, (a)-(c) are for the conic rod with taper ratio $\bar{\alpha}$ = 0.02 and (a)'-(c)' are for the same rod with taper ratio $\bar{\alpha}$ = 0.001. It is noted that the thick solid curves (—) for the lowest three mode shapes shown in Figures 6(a)-(c) agree with the solid curves (—) for the lowest three ones shown in Figures 5(a)-(c); similarly, the thick dashed curves (---) for the lowest

three mode shapes shown in Figures 6(a)'-(c)' also agree with the dashed curves (---) for the lowest three ones shown in Figures 5(a)-(c). Based on the foregoing reasonable results, it is believed that the presented theory should be reliable.

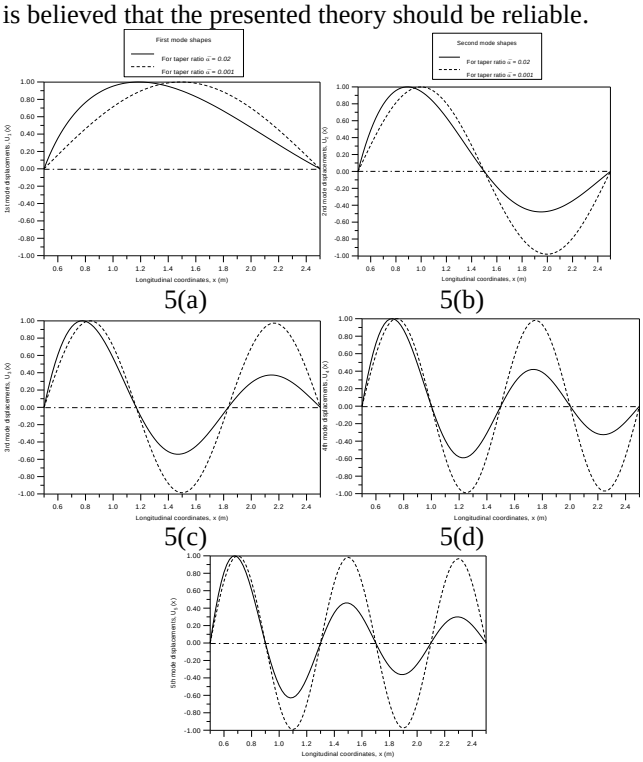

Figure 5 The lowest five mode shapes of the C-C rod (cf. Table 1) with taper ratios $\bar{\alpha} = d_\ell / L_\ell = 0.02$ (denoted by solid curves ——) and 0.001 (denoted by dashed curves ------): (a) 1st mode, (b) 2nd mode, (c) 3rd mode, (d) 4th mode and (e) 5th mode.

B. *Influence of total number of rod elements (n_e) for FEM*

As mentioned at the beginning of this section, the dimensions of the conic rod studied in current and subsequent subsections are the same as those of the rod with taper ratio $\bar{\alpha} = d_\ell / L_h = 0.01$ (i.e., case 2) shown in Table 1: $L_\ell = 5.0$ m, $L_s = 3.0$ m, $L = L_\ell - L_s = 2.0$ m, $d_s = 0.03$ m and $d_\ell = 0.05$ m. In order to find the influence of total number of rod elements, n_e, for the FEM on the lowest five natural frequencies ω_τ (rad/sec) of the conic rod with F-F, C-C, C-F and F-C boundary conditions, four subdivisions with $n_e = 20$, 30, 40 and 50 are studied here. The results are shown in Table 3, in which the exact natural frequencies are taken from cases 2 of Table 2 and the percentage errors in the parentheses of Table 3 are obtained from the formula, $\varepsilon\% = (\omega_{\tau\,FEM} - \omega_{\tau\,Exact}) \times 100\% / \omega_{\tau\,Exact}$, with $\omega_{\tau\,FEM}$ and $\omega_{\tau\,Exact}$ denoting the τ -th natural frequencies obtained from FEM and the presented exact method, respectively. From Table 3, it is seen that, among the four boundary conditions, the maximum percentage error for first natural frequencies obtained from FEM is less than 0.0166% (in C-C BC's) and that for the fifth ones is less than 0.4118% (in C-C BC's also) if $n_e = 50$. The last results further confirm the reliability of the presented exact method and the FEM, and total number of rod elements $n_e = 50$ is used for the finite element analysis in the next subsections because it leads to the small percentage errors.

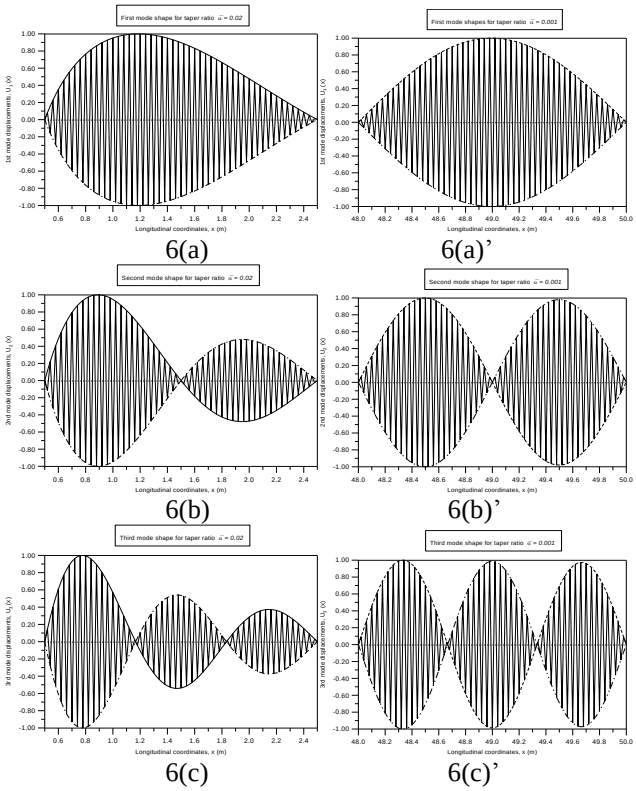

Figure 6 The envelopes for amplitudes of the lowest three mode displacements of the C-C rod (cf. cases 1 and 5 in Table 2) with taper ratios $\bar{\alpha} = d_\ell / L_\ell = 0.02$ (shown in (a)-(c)) and 0.001 (shown in (a)'-(c)'): (a)(a)' 1st mode, (b)(b)' 2nd mode, (c)(c)' 3rd mode.

C. *Effect of point masses*

In the foregoing subsections, all conic rods are the bare rods (without carrying any concentrated elements) with classical BC's (without any attachments at their ends). To show the effectiveness of the presented exact method for the more general cases, in the next subsections, all conic rods illustrated are the loaded rod (carrying arbitrary point masses or/and linear springs) with non-classical BC's (with a point mass or/and a linear spring at each free end). The loaded conic rod studied in this subsection is a free-clamped (F-C) one carrying 1, 3 and 5 point masses as shown in Figures 7(a), (b) and (c), respectively. In Figure 7(a) the single point mass with magnitude $\hat{m}_0 = m^*$ is located at free end of the rod with coordinate $x_0 = 3.0$ m, where $m^* = 20.140226$ kg is the reference mass. In Figure 7(b) the magnitude of each of the 3 point masses is given by $\hat{m}_i = \frac{1}{3} m^*$ ($i = 0, 1, 2$) located at $x_0 = 3.0$ m, $x_1 = 3.6$ m and $x_2 = 4.2$ m, respectively. It is similar to Figure 7(b) that the magnitude of each of the 5 point masses as shown in Figure 7(c) is given by $\hat{m}_i = \frac{1}{5} m^*$ ($i = 0, 1, 2, 3, 4$) located at $x_0 = 3.0$ m, $x_1 = 3.4$ m, $x_2 = 3.8$ m, $x_3 = 4.2$ m and $x_4 = 4.6$ m, respectively. For convenience of comparison, the lowest five nature frequencies of the corresponding bare F-C conic rod taken from case 2 of Table 2 are also listed at the final rows of Tables 4, 5 and 6, respectively, and the lowest five mode shapes are shown in Figure 8. It is noted that, in Figures 7, 9-11, the digits, 0, 1, 2, …, denote the numberings of nodes and the digits in parentheses, (1), (2), (3), …, denote those of

rod segments. As shown in column 4 of Table 4, the total numbers of rod segments for Figures 7(a), (b) and (c) are $n_s = 1$, 3 and 5, respectively. However, the total number of rod elements for the FEM is $n_e = 50$ in present and subsequent examples.

Table 3 Influence of total number of rod elements (n_e) on the lowest five natural frequencies ω_τ (rad/sec) of the conical rod (cf. case 2 in Table 1) with $L = 2.0$ m, $d_s = 0.03$ m, $d_\ell = 0.05$ m, $L_s = 3.0$ m and $L_\ell = 5.0$ m, by using FEM.

BCS	n_e	Natural frequencies, ω_τ (rad/sec)				
		ω_1	ω_2	ω_3	ω_4	ω_5
FF	20	8276.15 *(0.08%)	16296.17 (0.39%)	24479.93 (0.91%)	32831.31 (1.63%)	41390.83 (2.56%)
	30	8272.15 (0.03%)	16260.55 (0.17%)	24357.19 (0.40%)	32537.73 (0.72%)	40814.32 (1.13%)
	40	8270.75 (0.02%)	16248.09 (0.09%)	24314.27 (0.22%)	32435.19 (0.40%)	40613.13 (0.63%)
	50	8270.10 (0.01%)	16242.32 (0.06%)	24294.41 (0.14%)	32387.78 (0.26%)	40520.14 (0.40%)
	#Exact	**8268.95**	**16232.06**	**24259.13**	**32303.56**	**40355.09**
CC	20	8070.63 (0.10%)	16191.04 (0.41%)	24411.35 (0.92%)	32782.06 (1.65%)	41354.05 (2.58%)
	30	8066.01 (0.04%)	16154.14 (0.18%)	24286.56 (0.41%)	32485.56 (0.73%)	40773.55 (1.14%)
	40	8064.40 (0.02%)	16141.23 (0.10%)	24242.96 (0.23%)	32382.08 (0.41%)	40571.12 (0.64%)
	50	8063.65 (0.01%)	16135.26 (0.06%)	24222.80 (0.14%)	32334.24 (0.26%)	40477.60 (0.41%)
	Exact	**8062.32**	**16124.65**	**24186.97**	**32249.30**	**40311.62**
CF	20	3246.80 (0.05%)	11902.70 (0.25%)	20158.51 (0.66%)	28487.52 (1.29%)	36975.70 (2.12%)
	30	3245.72 (0.02%)	11885.71 (0.11%)	20083.88 (0.29%)	28285.43 (0.57%)	36547.87 (0.93%)
	40	3245.34 (0.01%)	11879.77 (0.06%)	20057.82 (0.16%)	28214.94 (0.32%)	36398.79 (0.52%)
	50	3245.17 (0.00%)	11877.02 (0.04%)	20045.77 (0.10%)	28182.36 (0.20%)	36329.93 (0.33%)
	Exact	**3244.8615**	**11872.14**	**20024.36**	**28124.51**	**36207.72**
FC	20	4893.82 (0.00%)	12467.86 (0.19%)	20493.28 (0.60%)	28718.60 (1.21%)	37145.69 (2.04%)
	30	4894.03 (0.00%)	12454.68 (0.08%)	20425.28 (0.26%)	28526.37 (0.54%)	36731.58 (0.90%)
	40	4894.10 (0.00%)	12450.06 (0.04%)	20401.47 (0.15%)	28459.12 (0.30%)	36586.84 (0.51%)
	50	4894.13 (0.00%)	12447.92 (0.03%)	20390.44 (0.09%)	28428.00 (0.19%)	36519.90 (0.32%)
	Exact	**4894.20**	**12444.11**	**20370.84**	**28372.70**	**36400.99**

Exact solutions obtained from cases 2 in Table 2.

* Percentage errors obtained from the formula: $\varepsilon\% = (\omega_{\tau\,FEM} - \omega_{\tau\,Exact}) \times 100\% / \omega_{\tau\,Exact}$ with $\omega_{\tau\,FEM}$ and $\omega_{\tau\,Exact}$ denoting the τ -th natural frequencies obtained from FEM and the presented exact method.

Table 4 Influence of point masses (each with magnitude $\hat{m}_i = m^* / N_{\hat{m}}$) on the lowest five natural frequencies of the F-C conic rod (cf. Figure 7), with $N_{\hat{m}}$ denoting total number of point masses (for each case) and $m^* = 20.140226$ kg denoting reference mass.

$N_{\hat{m}}$	$\hat{m}_i$	n_s / n_e	Method	Natural frequencies, ω_τ (rad/sec)				
				ω_1	ω_2	ω_3	ω_4	ω_5
1	m^*	1	Exact	2250.84	8499.78	16348.09	24336.53	32361.62
		50	FEM	2250.82	8501.18	16358.85	24372.57	32446.86
3	$\frac{1}{3}m^*$	3	Exact	2838.52	7236.49	11244.68	21889.53	28686.07
		50	FEM	2838.47	7236.69	11245.79	21913.29	28738.89
5	$\frac{1}{5}m^*$	5	Exact	3035.78	7840.23	12531.10	16637.64	20473.61
		50	FEM	3035.73	7840.52	12532.70	16641.44	20481.00
Bare rod		1	*Exact	**4894.20**	**12444.11**	**20370.84**	**28372.70**	**36400.99**

* The exact values for the lowest five natural frequencies of the bare F-C rod taken from case 2 of Table 2

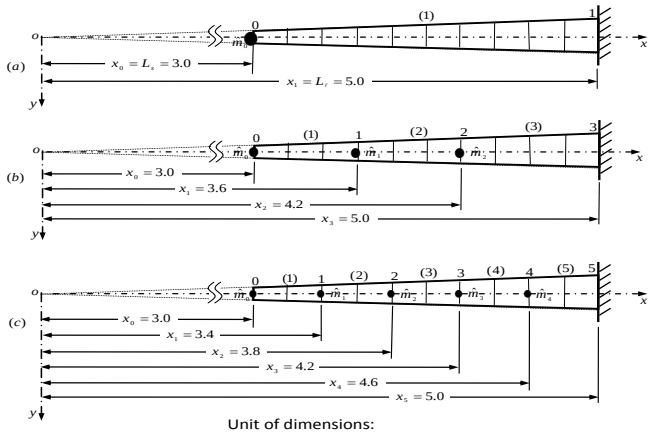

Figure 7 The F-C conic rod (cf. case 2 of Table 1) carrying: (a) 1 point mass with magnitude $\hat{m}_0 = m^*$ located at $x_0 = 3.0$ m; (b) 3 point masses each with magnitude $\hat{m}_i = \frac{1}{3}m^*$ ($i = 0, 1, 2$) located at $x_0 = 3.0$ m, $x_1 = 3.6$ m and $x_2 = 4.2$ m, respectively; (c) 5 point masses each with magnitude $\hat{m}_i = \frac{1}{5}m^*$ ($i = 0, 1, 2, 3, 4$) located at $x_0 = 3.0$ m, $x_1 = 3.4$ m, $x_2 = 3.8$ m, $x_3 = 4.2$ m and $x_4 = 4.6$ m, respectively.

From Table 4, one sees that the influence on the 1st natural frequency of the loaded rod decreases with the increase of total number of point masses, $N_{\hat{m}}$, carried by the rod (for each case), and this trend is reverse for the influence on the 4th and 5th ones. The last phenomenon has something to do with: (i) the summation of the point masses for either Figure 7(a), (b) or (c) is constant, i.e., $\sum_{j=1}^{N_{\hat{m}}} \hat{m}_j = m^*$, (ii) the point mass at free end of either Figure 7(a), (b) or (c) is located at the crest of each mode shape shown in Figure 8, (iii) the effect of concentrated mass is greater than that of the distributed masses and (iv) the relative positions between the intermediate point masses (in Figure 7) and the intermediate nodes (or crests) of the associated mode shapes (in Figure 8). It is seen that all numerical results obtained from the presented exact method are very close to those obtained from the conventional FEM.

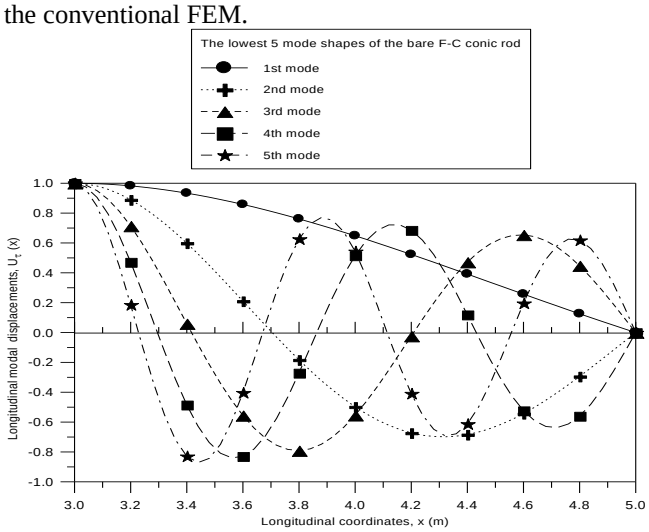

Figure 8 The lowest five mode shapes of the bare F-C conic rod (with corresponding natural frequencies shown in case 2 of Table 2).

D. *Effect of linear springs*

The conic rod studied in this subsection (Figure 9) is the same as that studied in the last subsection (Figure 7), but all the point masses are replaced by the linear springs each with stiffness $\hat{k}_i = k^* / N_{\hat{k}}$ ($i = 0, 1, 2, \ldots$), where $N_{\hat{k}}$ denotes the total number of linear springs for each case. Because the locations for the linear springs in Figure 9 are the same as those for the point masses in Figure 7, so are the numberings of nodes and rod segments. The results are shown in Table 5. It is found that the trends of the lowest five natural frequencies of the loaded conic rods given in Table 5 are opposite to those given in Table 4, because the effect of the linear springs attached to the rod (in Figure 9) are opposite to that of the point masses carried by the same rod shown in Figure 7. One of the main difference between the effect of point masses (cf. Table 4) and that of linear springs (cf. Table 5) is that the point masses reduce the lowest five natural frequencies of the conic rod significantly as one may see from Table 4, but the effect of linear springs is significant for the first natural frequency only and is negligible for the 2nd to 5th ones as one may see from Table 5. In other words, the overall effect of linear springs is much smaller than that of the point masses for the present example.

Table 5 Influence of linear springs (each with stiffness $\hat{k}_i = k^* / N_{\hat{k}}$) on the lowest five natural frequencies of the F-C conic rod (cf. Figure 9), with $N_{\hat{k}}$ denoting total number of linear springs and $k^* = 1.3805728 \times 10^8$ N/m denoting reference stiffness.

$N_{\hat{k}}$	$\hat{k}_i$	n_s / n_e	Method	Natural frequencies, ω_τ (rad/sec)				
				ω_1	ω_2	ω_3	ω_4	ω_5
1	k^*	1	Exact	6132.77	13271.36	20934.92	28792.88	36733.87
		50	FEM	6133.10	13276.36	20956.47	28850.89	36856.24
3	$\frac{1}{3}k^*$	3	Exact	6013.96	12900.66	20620.58	28683.31	36551.71
		50	FEM	6014.13	12905.03	20641.06	28740.53	36672.12
5	$\frac{1}{5}k^*$	5	Exact	5862.64	12844.06	20614.73	28548.82	36552.89
		50	FEM	5862.75	12848.33	20635.11	28605.25	36673.43
Bare rod		1	Exact	**4894.20**	**12444.11**	**20370.84**	**28372.70**	**36400.99**

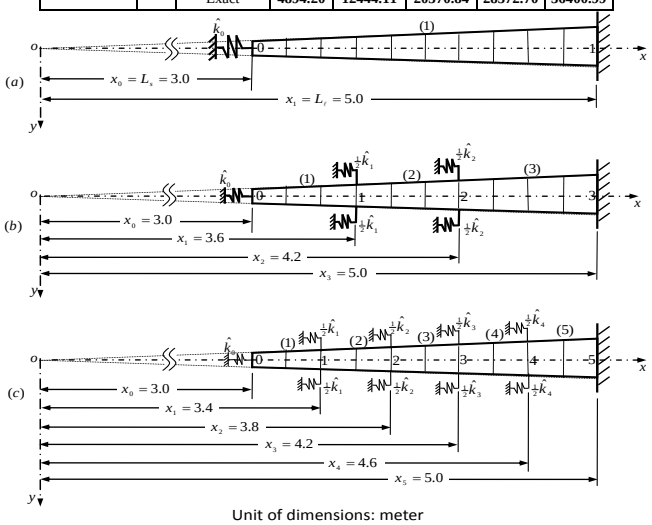

Figure 9 The F-C conic rod carrying: (a) 1 linear spring with stiffness $\hat{k}_0 = k^*$; (b) 3 linear springs each with stiffness $\hat{k}_i = \frac{1}{3}k^*$ ($i = 0, 1, 2$); (c) 5 linear springs each with stiffness $\hat{k}_i = \frac{1}{5}k^*$ ($i = 0, 1, 2, 3, 4$), where $k^* = 1.3805728 \times 10^8$ N/m (reference stiffness). The positions of the linear springs $\hat{k}_i$ are identical to those of the corresponding point masses $\hat{m}_i$ shown in the caption of Figure 7.

Table 6 Influence of both point masses $\hat{m}_i$ and linear springs $\hat{k}_i$ (each with $\hat{m}_i = m^* / N_{\hat{m}}$ and $\hat{k}_i = k^* / N_{\hat{k}}$) on the lowest five natural frequencies of the F-C conic rod (cf. Figure 10), with $N_{\hat{m}} = N_{\hat{k}}$ denoting total number of point masses (or linear springs), $m^* = 20.140226$ kg and $k^* = 1.3805728 \times 10^8$ N/m.

$N_{\hat{m}} = N_{\hat{k}}$	$\hat{m}_i$ / $\hat{k}_i$	n_s / n_e	Method	Natural frequencies, ω_τ (rad/sec)				
				ω_1	ω_2	ω_3	ω_4	ω_5
1	m^*	1	Exact	3269.30	8543.23	16353.91	24338.27	32362.36
	k^*	50	FEM	3269.27	8544.61	16364.66	24374.32	32447.59
3	$\frac{1}{3}m^*$	3	Exact	3559.44	7548.14	11455.19	21906.26	28699.86
	$\frac{1}{3}k^*$	50	FEM	3559.38	7548.36	11456.35	21930.02	28752.66
5	$\frac{1}{5}m^*$	5	Exact	3669.93	8099.98	12703.30	16775.09	20584.53
	$\frac{1}{5}k^*$	50	FEM	3669.87	8100.31	12704.97	16778.97	20592.04
Bare rod		1	Exact	**4894.20**	**12444.11**	**20370.84**	**28372.70**	**36400.99**

E. *The combined effect of both point masses and linear springs*

The conic rod studied in this subsection is also the same as the one studied in the last two subsections, but both the point mass $\hat{m}_i$ in Figure 7 and the linear spring $\hat{k}_i$ in Figure 9 are attached to the same corresponding node *i* in Figure 10. Because the locations and magnitudes of the point masses and linear springs studied in this subsection are the same as the corresponding ones given in the last two subsections, the overall effect for the combination of point masses and linear springs should be the net effect of the point masses only and the linear springs only. Since, as shown in the last subsection, the effect of point masses only are much greater than that of linear springs only, it is under expectation that the net effect of both point masses and linear springs is similar to the effect of the point masses only. This is one of the reasons why, in Table 6, the first natural frequency is significantly influenced by the attachment of both point masses and linear springs, but the 2nd to 5th natural frequencies of the loaded rod are very close to those given in Table 4 for the point masses only.

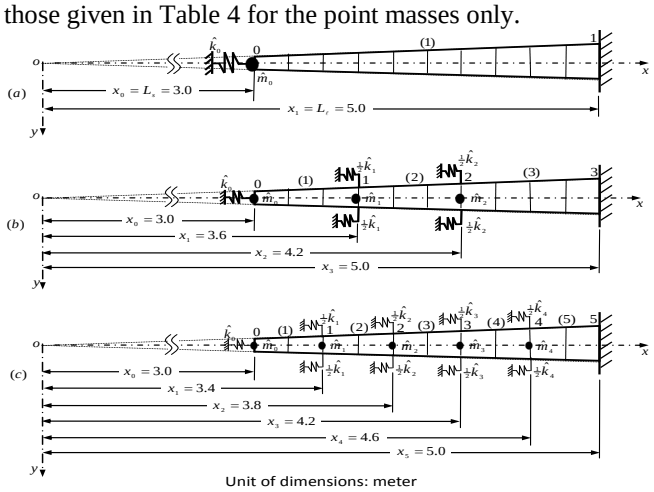

Figure 10 The F-C conic rod carrying: (a) 1 point mass $\hat{m}_0$ and 1 linear spring $\hat{k}_0$ (with $\hat{m}_0 = m^*$ and $\hat{k}_0 = k^*$); (b) 3

point masses $\hat{m}_i$ and 3 linear springs $\hat{k}_i$ (with $\hat{m}_i = \frac{1}{3}m^*$ and $\hat{k}_i = \frac{1}{3}k^*$, $i = 0, 1, 2$); (c) 5 point masses $\hat{m}_i$ and 5 linear springs $\hat{k}_i$ (with $\hat{m}_i = \frac{1}{5}m^*$ and $\hat{k}_i = \frac{1}{5}k^*$, i = 0, 1, 2, 3, 4), where $m^* = 20.140226$ kg and $k^* = 1.3805728 \times 10^8$ N/m. The positions of the point masses $\hat{m}_i$ (and linear springs $\hat{k}_i$) are identical to those of the corresponding point masses $\hat{m}_i$ shown in the caption of Figure 7.

F. Free vibration analysis of an elastic-support F-F conic rod carrying multiple point masses

The final example studied in this paper is a free-free (F-F) conic rod elastically supported by four identical linear springs each with stiffness $\hat{k}_i = k^*/N_{\hat{k}}$ as shown in Figure 11. The dimensions and physical constants of the conic rod are the same as those for the last examples. From Figure 11 one sees that the conic rod is supported by two springs at its two ends and by another two springs at two intermediate nodes located at $x = 3.0$, 3.6, 4.4 and 5.0m, respectively. The lowest five natural frequencies for the elastic-support rod carrying 0, 2 and 3 point masses are shown in Table 7, where $\hat{m}_i = m^*/N_{\hat{m}}$ with $N_{\hat{m}}$ denoting the total number of point masses for Figure 11(b) or (c). The lowest five mode shapes for the elastic-support rod carrying 0 point mass (cf. Figure 11 (a)) are shown in Figure 12. From Table 7 and Figure 12 one sees that the natural frequency for the mode shape denoted by the dashed line with circles (—○ —) is $\omega_0^{(a)} = 2581.6955$ rad/sec. Because the longitudinal deformation of this mode shape is very small and the corresponding natural frequency $\omega_0^{(a)}$ is very close to $\omega_{\text{rig}}^{(a)} = \sqrt{k^*/m^*}$ = 2618.1679 rad/sec, it is called the quasi rigid-body mode in this paper. Since the reference mass $m^* = 20.140226$ kg is equal to the total mass of the conic rod and the summation of the stiffness of the four linear springs is equal to the reference stiffness $k^* = 1.3805728 \times 10^8$ N/m, the true rigid-body natural frequency of the vibrating system shown in Figure 11(a) is given by $\omega_{\text{rig}}^{(a)} = \sqrt{k^*/m^*}$ if the conic rod is rigid. Similarly, the true rigid-body natural frequency for the vibrating system shown in Figure 11(b) or (c) is given by $\omega_{\text{rig}}^{(b)} = \omega_{\text{rig}}^{(c)} = \sqrt{k^*/(2m^*)}$ = 1851.3242 rad/sec, which is very close to the quasi rigid-body natural frequencies listed in Table 7 ($\omega_0^{(b)} = 1811.6539$ or $\omega_0^{(c)} = 1829.7592$ rad/sec). It is noted that the summation of the point masses in Figure 11(b) or (c) is equal to the reference mass m^*, thus, the effective mass of the vibrating system shown in Figure 11(b) or (c) is equal to $2m^*$.

From Table 7 one also finds that the lowest four elastic natural frequencies of the elastic- support conic rod shown in Figure 11(a) are very close to the corresponding ones of the bare rod listed in the final row of Table 7 except the first one ω_1. Now, one may compare the lowest four elastic natural frequencies of the vibrating system shown in Figure 11(b) or (c) with those shown in Figure 11(a), because the only difference between them is the total number of point masses. It is under expectation that the values of ω_1 to ω_4 for the conic rod shown in Figure 11(b) or (c) are much lower than those shown in Figure 11(a), because there exist 2 or 3 point masses for the rod in Figure 11(b) or (c), and no point mass for the rod in Figure 11(a). In addition to the lowest four elastic natural frequencies, the lowest three elastic mode shapes of the loaded rod are compared with the corresponding ones of the bare rod in Figure 13. In which, the mode shapes of the loaded rod are denoted by the solid curves (——) and those of the bare rod by the dashed curves (------), besides, the 1st, 2nd and 3rd mode shapes are represented by the symbols, ●, ✚ and ▲, respectively. Because the corresponding natural frequencies are much different from each other (cf. Table 7) so are the corresponding mode shapes shown in Figure 13.

Table 7 Influence of point masses $\hat{m}_i$ on the lowest five natural frequencies of the F-F conic rod elastically supported by four linear springs $\hat{k}_i$ (each with stiffness $\hat{k}_i = k^*/4$) (cf. Figure 11) with $k^* = 1.3805728 \times 10^8$ N/m and $m^* = 20.140226$ kg.

$N_{\hat{m}}$	$\hat{m}_i$	n_s / n_e	Method	Natural frequencies, ω_τ (rad/sec)				
				* ω_0	ω_1	ω_2	ω_3	ω_4
0	–	3	Exact	2581.69	8885.13	16499.83	24558.71	32507.80
		50	FEM	2581.76	8886.62	16510.65	24595.39	32593.63
2	$\frac{1}{2}m^*$	5	Exact	1811.65	6537.30	13403.10	20895.76	25071.42
		50	FEM	1811.67	6537.68	13405.91	20919.52	25102.66
3	$\frac{1}{3}m^*$	6	Exact	1829.75	5609.92	9847.18	21884.29	25126.20
		50	FEM	1829.77	5610.10	9848.21	21908.58	25156.75
Bare rod		1	Exact	–	**8268.95**	**16232.06**	**24259.13**	**32303.56**

* Quasi rigid-body natural frequencies.

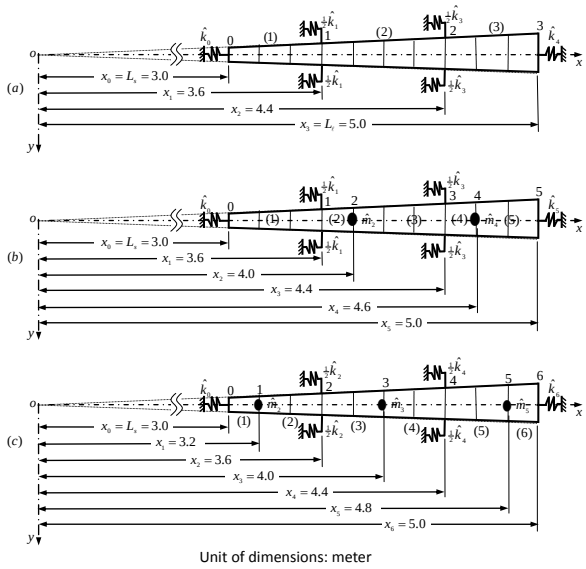

Figure 11 The F-F conic rod supported by four linear springs (each with stiffness $\hat{k}_i = \frac{1}{4}k^*$ ($i = 0, 1, 2, 3$) located at $x = 3.0$, 3.6, 4.4 and 5.0m, respectively, and carrying: (a) no point mass; (b) 2 point masses each with magnitude $\hat{m}_i = \frac{1}{2}m^*$ ($i = 1, 2$) located at $x_1 = 3.8$ m and $x_2 = 4.6$ m, respectively; (c) 3 point masses each with magnitude $\hat{m}_i = \frac{1}{3}m^*$ ($i = 1, 2, 3$) located at $x_1 = 3.2$ m, $x_2 = 4.0$ m and $x_3 = 4.8$ m, respectively.

VIII. CONCLUSIONS

1 In addition to the computation efficiency, the accuracy of

the numerical results of an approximate method is also an important factor affecting its availability. Therefore, the presented exact method for obtaining the natural frequencies and associated mode shapes of the longitudinal-vibration general conic rod with or without carrying any number of point masses and/or linear springs will be significant for evaluating the accuracy of various existing approximate methods concerned (such as FEM).

2 The formulation of this paper is very flexible, because: (i) the locations of the concentrated elements on the rod are arbitrary; (ii) the total number of concentrated elements attached to the rod is also arbitrary including zero; (iii) each node may be attached by either a point mass or a linear spring or both of them.

3 For free vibrations of the general conic rods carrying any number of point masses and/or linear springs with various (classical or non-classical) boundary conditions, the modified numerical assembly method introduced in this paper significantly reduces the difficulty for obtaining the exact solution of the problem.

4 Since all Bessel functions are replaced by the associated trigonometric functions in this paper, much difficulty concerning the differentiations and computer coding of the Bessel functions is removed.

5 For a general conic rod with clamped-clamped (C-C) boundary conditions, the taper ratio $\overline{\alpha} = d_\ell / L_\ell$ does not affect its lowest several natural frequencies but significantly influences the associated mode shapes, where d_ℓ and L_ℓ denote the diameter and axial coordinate at the larger end of the conic rod, respectively. For each mode shape, the larger the taper ratio of the rod, the larger the divergence between the local maximum mode displacement near its smaller end and that near its larger end.

6 For a uniform rod, the natural frequencies of the clamped-free (C-F) one are the same as those of the free-clamped (F-C) one. However, the last statement is incorrect for a conic rod, because the natural frequencies of the C-F conic rod are different from those of the F-C conic rod, and the divergence between them is dependent upon the magnitude of taper ratio $\overline{\alpha} = d_\ell / L_\ell$.

7 For the conic rod studied in this paper, if the *reference mass* is defined by $m^* = \frac{1}{3}\rho(A_\ell L_\ell - A_s L_s)$ and the *reference stiffness* defined by $k^* = EA_{ave}/L$, where A_s and L_s are the cross-sectional area and axial coordinate at smaller end, A_ℓ and L_ℓ are those at larger end of the conic rod, respectively, $L = L_\ell - L_s$ is the rod length and $A_{ave} = (A_\ell + A_s)/2$ is the average cross-sectional area, and if the summation of point masses is equal to the reference mass (i.e. $\sum \hat{m}_j = m^*$) and that of stiffness of linear springs is equal to the reference stiffness (i.e., $\sum \hat{k}_j = k^*$), then the effect on the lowest five natural frequencies of the F-C loaded rod carrying point masses ($\hat{m}_j$) only are much greater than that carrying linear springs ($\hat{k}_j$) only. Because of the last phenomenon, the influence on the free vibration characteristic of a loaded rod carrying both point masses and linear springs are mainly dependent on the point masses.

8 For a free-free (F-F) rod supported by arbitrary linear springs $\hat{k}_j$ and carrying a number of point masses $\hat{m}_j$, there exists a quasi rigid-body natural frequency ω_0 to be very close to the true one given by $\omega_{\text{rig}} = \sqrt{K/(M + m_b)}$, where m_b is total mass of the rod, $K = \sum_{j=1}^{N_{\hat{k}}} \hat{k}_j$ and $M = \sum_{j=1}^{N_{\hat{k}}} \hat{m}_j$ with $\hat{m}_j$ and $N_{\hat{m}}$ denoting the total number of linear springs and point masses, respectively.

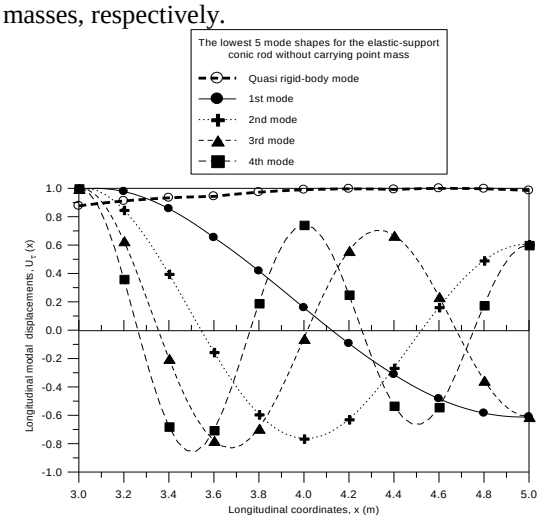

Figure 12 The lowest five mode shapes of the elastic-support F-F conic rod without carrying any point mass as shown in Figure 11(a).

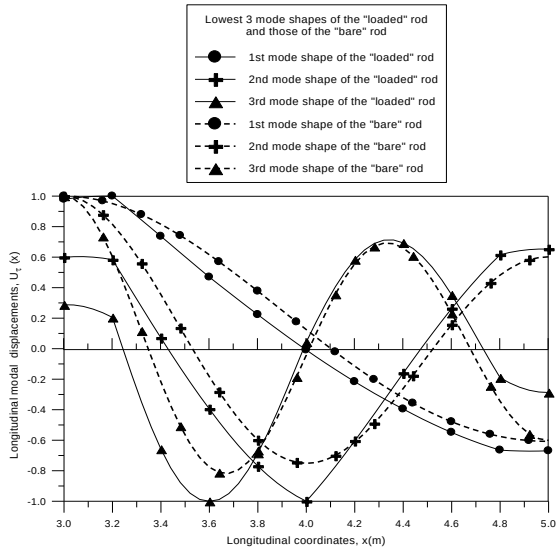

Figure 13 Comparison between the lowest three elastic mode shapes of the loaded conic rod shown in Figure 11(c) (denoted by the solid curves, ——) and those of the associated bare rod (denoted by the dashed curves, -----). The symbols, ●, ✚ and ▲, represent the 1st, 2nd and 3rd modes, respectively.

APPENDIX A CROSS-SECTIONS FOR SPECIFIC CONIC ROD WITH AREA VARIATION $A(x) = (ax + b)^4$

In references [3, 4, 5], the area variation of the conic rods is to take the specific function

$$A(x) = (ax + b)^4 \tag{A.1}$$

Thus, the radius variation of the conic rods is given by

$$r(x)=\sqrt{A(x)/\pi}=(ax+b)^2/\sqrt{\pi} \qquad \text{(A.2)}$$

From the numerical examples illustrated in reference [4], one sees that a = 1, 2; b = 1 and L = 1. Therefore, the radius variation $r(x)$ along the longitudinal x-axis is shown in Fig, A1 for the cases of a = 1 (denoted by the solid curves, ——) and a = 2 (denoted by the dashed curves, ------). From the figure, it is seen that revolution of the inclined solid curve $\overline{AB}$ about the horizontal x-axis will generate the longitudinal (lateral) surface of the conic rod denoted by the solid lines (——). Similarly, revolution of the inclined dashed curve $\overline{AB'}$ about the horizontal x-axis will generate that of the conic rod denoted by the dashed lines (------).

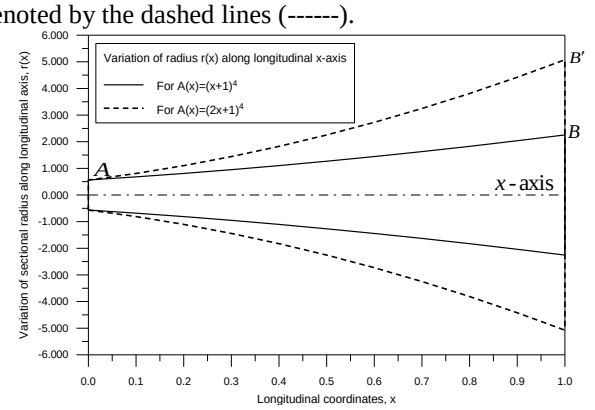

Figure A1 Profiles of longitudinal cross-sections of the specific conic rods with area variations $A(x)=(x+1)^4$ (denoted by the solid lines, ——) and $A(x)=(2x+1)^4$ (denoted by the dashed lines, -------).

APPENDIX B EXACT NATURAL FREQUENCIES AND MODE SHAPES OF A UNIFORM ROD

From reference [7] one may derive the next formulas for the exact natural frequencies and mode shapes of a longitudinal-vibration uniform rod with various boundary conditions:

(i) F-F rod and C-C rod

The exact natural frequencies for the longitudinal vibrations of a uniform rod with free-free (F-F) boundary conditions are the same as those with clamped-clamped (C-C) ones. They are given by

$$\beta_\tau=\tau\pi/L \quad (\tau=0,1,2,3,\ldots,\infty) \qquad \text{(A.3)}$$

$$\omega_\tau=\frac{\beta_\tau L}{L}\sqrt{\frac{E}{\rho}}=\frac{\tau\pi}{L}\sqrt{\frac{E}{\rho}} \quad (\tau=0,1,2,3,\ldots,\infty) \qquad \text{(A.4)}$$

However, the associated mode shapes are different from each other and given by

$$U_\tau(x)=A_\tau\cos(\tau\pi x/L) \quad (\tau=0,1,2,3,\ldots,\infty) \qquad \text{(A.5)}$$

for F-F rod, and

$$U_\tau(x)=A_\tau\sin(\tau\pi x/L) \quad (\tau=1,2,3,\ldots,\infty) \qquad \text{(A.6)}$$

for C-C rod.

Since $\tau=0$ represents the rigid-body mode, the formulas given by Equations (A.3) and (A.4) with $\tau=0$ are correct only for the F-F rod.

(ii) C-F rod

The exact natural frequencies and mode shapes of a uniform rod with clamped-free (C-F) boundary conditions are given by

$$\beta_\tau=\frac{\tau\pi}{2L} \quad (\tau=1,3,5,\ldots,\infty) \qquad \text{(A.7)}$$

$$\omega_\tau=\frac{\beta_\tau L}{L}\sqrt{\frac{E}{\rho}}=\frac{\tau\pi}{2L}\sqrt{\frac{E}{\rho}} \quad (\tau=1,3,5,\ldots,\infty)$$

$$\rightarrow \omega_s=\frac{(2s-1)\pi}{2L}\sqrt{\frac{E}{\rho}} \quad (s=1,2,3,\ldots,\infty) \qquad \text{(A.8)}$$

$$U_\tau(x)=A_\tau\sin\left(\frac{\tau\pi x}{2L}\right) \quad (\tau=1,3,5,\ldots,\infty)$$

$$\rightarrow U_s(x)=A_s\sin\left(\frac{(2s-1)\pi x}{2L}\right) \quad (s=1,2,3,\ldots,\infty) \qquad \text{(A.9)}$$

(iii) F-C rod

The exact natural frequencies and mode shapes for a uniform rod with free-clamped (F-C) boundary conditions are given by

$$\beta_\tau=\frac{\tau\pi}{2L} \quad (\tau=1,3,5,\ldots,\infty) \qquad \text{(A.10)}$$

$$\omega_\tau=\frac{\beta_\tau L}{L}\sqrt{\frac{E}{\rho}}=\frac{\tau\pi}{2L}\sqrt{\frac{E}{\rho}} \quad (\tau=1,3,5,\ldots,\infty)$$

$$\rightarrow \omega_s=\frac{(2s-1)\pi}{2L}\sqrt{\frac{E}{\rho}} \quad (s=1,2,3,\ldots,\infty) \qquad \text{(A.11)}$$

$$U_\tau(x)=A_\tau\cos\left(\frac{\tau\pi x}{2L}\right) \quad (\tau=1,3,5,\ldots,\infty)$$

$$\rightarrow U_s(x)=A_s\cos\left(\frac{(2s-1)\pi x}{2L}\right) \quad (s=1,2,3,\ldots,\infty) \qquad \text{(A.12)}$$

It is noted that, the frequency parameters β_τ given by Equation (A.10) are the same as those given by Equation (A.7), but the corresponding mode shapes $U_\tau(x)$ defined by Equation (A.12) are different from those defined by Equation (A.9).

ACKNOWLEDGMENT

This work was supported by the National Science Council, the Republic of China, under contract No. NSC 102-2221-E-022-007.

REFERENCES

[1] N. M. Auciello, "Transverse vibration of a linearly tapered cantilever beam with tip mass of rotary inertia and eccentricity," *Journal of Sound and Vibration*, vol. 194, 1996, pp. 25-34.

[2] J. S. Wu, and C.T. Chen, "An exact solution for the natural frequencies and mode shapes of an immersed elastically restrained wedge beam carrying an eccentric tip mass with mass moment of inertia," *Journal of Sound and Vibration*, vol. 286, 2005, pp. 549-568.

[3] S. Abrate, "Vibration of non-uniform rods and beams," *Journal of Sound and Vibration*, vol. 185, 1995, pp. 703-716.

[4] B. M. Kumar, and R.I. Sujith, "Exact solutions for the longitudinal vibration of non-uniform rods," *Journal of Sound and Vibration*, vol. 207, 1997, pp. 721-729.

[5] Q. S. Li, "Exact solutions for free longitudinal vibration of non-uniform rods," *Journal of Sound and Vibration*, vol. 234, 2000, pp. 1-19.

[6] F.D. Faires, and R.L. Burden, *Numerical Methods*, PWS, Boston, 1993.

[7] L. Meirovitch, *Analytical Methods in Vibrations*, the Macmillan Company, London, 1967.

[8] C. R., Wylie, JR, *Advance Engineering Mathematics*, 3rd edition, McGraw-Hill, New York, 1966.

[9] H. B. Dwight, *Tables of Integrals and Other Mathematical Data*, Massachusetts Institute of Technology, 3rd Ed., 1957, pp.180.

[10] J. S. Przemieniecki, *Theory of Matrix Structural Analysis*, McGraw-Hill, New York, 1968.